A METHOD FOR MULTIPATH DETECTION AND MITIGATION IN RAILWAY CONTROL APPLICATIONS[1]

Alessandro Neri[a], Veronica Palma[a], Francesco Rispoli[b], Sam Pullen[c], Shiwen Zhang[c], Sherman Lo[c], and Per Enge[c]

[a] RadioLabs, Corso d'Italia 19, Rome, Italy
[b]Ansaldo STS, Genoa, Italy
[c]Stanford University, Stanford, CA, USA

BIOGRAPHIES

Alessandro NERI is Full Professor in Telecommunications at the Engineering Department of the ROMA TRE University. In 1977 he received the Doctoral Degree in Electronic Engineering from "Sapienza" University of Rome. In 1978 he joined the Research and Development Department of Contraves Italiana S.p.A. where he gained a specific expertise in the field of radar signal processing and in applied detection and estimation theory, becoming the chief of the advanced systems group. In 1987 he joined the INFOCOM Department of "Sapienza" University of Rome as Associate Professor in Signal and Information Theory. In November 1992 he joined the Electronic Engineering Department of ROMA TRE University as Associate Professor in Electrical Communications, and became Full Professor in Telecommunications in September 2001. His research activity has mainly been focused on information theory, signal theory, signal and image processing, location and navigation technologies, and their applications to both telecommunications systems and remote sensing.

Since December 2008, Prof. Neri is the President of the RadioLabs Consortium, a non-profit Research Center created in 2001 to promote tight cooperation on applied research programs between universities and industries.

Veronica Palma received the Laurea (Master of Science) in Electronic Engineering from Università degli Studi Roma Tre, Rome, Italy, in May 2007. In May 2011, she discussed her Ph.D. thesis entitled "Distributed Video Coding of 3D Sources", at the "Biomedical electronics, Electromagnetics and Telecommunications" doctoral school in Engineering of the University "Roma Tre". From March 2013 to June 2014 she attended I Level Master on "Full HD, 3D Immersive and Interactive Video in Advanced Convergence and Cross-media Environments.''

She is now a researcher at RadioLabs, where she has been involved in international and national projects mostly based on satellite navigation applications. Her research interests are mainly focused on: routing protocol optimization in mobile networks, network coding, and satellite navigation.

Francesco RISPOLI has joined Ansaldo STS in 2011 as responsible for Satellite and Telecommunication technologies. He is Director General of RadioLabs and Director of Galileo Services board. Previously, he has been with Telespazio (2005-2011) as Chief of New Initiatives and by 1983 to 2005 with Alenia Spazio (now Thales Alenia Space) where he served various positions as responsible for R&D and Institutional programs, Vice President of Multimedia business unit and General Manager of EuroSkyWay. He started his carrier in 1980 with Contraves Italiana as technical engineer in the antenna department. In 1978 he received the Doctoral Degree in Electronic Engineering from the Polytechnic of Turin and in 1980 a post-graduate Master in Applied Electromagnetism from the University of Roma La Sapienza. He is currently involved into the Pilot project ERSAT (ERTMS over SATELLITE) in Sardinia Region and other related projects such as 3InSat and NGTC. He is also contributing to EGNOS-R (railways) interface with Local Augmentation networks and the certification process.

[1] This work has been developed under the grant of the "RHINOS" project of the H2020-Galileo-GSA-2014-2015/H2020-Galileo-2015-1 Program (Project Number 687399).

ABSTRACT

GNSS is expected to revolutionize train control systems by providing an efficient alternative to determine the train position along the track. However, GNSS is particularly vulnerable in the rail environment because of the presence of multipath in stations and at many locations along the track. Therefore, particular attention must be placed in assessing and evaluating multipath errors introduced by GNSS when using GNSS to replace physical balises with virtual balises.

In this paper we investigate a multipath detector based on the analysis of the double differences of pseudoranges provided by two GNSS receivers on board a train making use of two different antennas.

This research, is developed within the RHINOS project co-funded by the GSA that is contributing to the roadmap for introducing GNSS into the European Train Management System (ERTMS).

Index Terms— Railway applications, PVT estimation, Protection Level, Hazardous Misleading Information, ERTMS

1. INTRODUCTION

GNSS represents a most wanted "wheel of change" for train control systems for a long time, as it can provide reliable, safe and cost efficient train positioning for managing railway traffic. Train positioning is a safety critical function impacting directly on the safety (and also performance) of the entire train control system. In the USA, GNSS is already being adopted by the majority of the PTC (Positive Train Control) systems being deployed [1]. In Europe, GNSS has been included recently into the ERTMS (European Train Management System) evolution roadmap envisaged by ERA (European Railways Agency), which has identified GNSS as one of the "Game Changers" for improving the competitiveness of ERTMS [2]. The benefit of GNSS is the replacement of the track-side beacons (balises) necessary to periodically reset the onboard odometer's confidence error, which increases with the distance travelled. Virtual balises, a concept preconized in the early 1990s [3], allows GNSS to support the legacy ERTMS principle of operation and, in the longer term, will drive the adoption of GNSS for train integrity monitoring and moving block operations, making the train "autonomous" from the track circuits.

In the short term, GNSS will provide three benefits. The first is to guarantee backward compatibility with existing physical-balise-based tracks and networks. The second is to lower the cost of maintaining and operating ERTMS. The third is the reduction of mission start time, since the train has to be operated under driver responsibility until ERTMS obtains full supervision of the train. Considering these benefits, RFI (Rete Ferroviaria Italiana), an early adopter of ERTMS and one of the largest European rail infrastructure managers, has accelerated their plans, launched in 2012 and involving also DB-Netz from Germany, for contributing to the certification of GNSS-based ERTMS applications as part of the modernization of local and regional lines in Italy [4].

With this aim in mind, RFI has nominated a Technical Committee to evaluate the risk of introducing GNSS according to European Rule 402-2013, as required by safety certification procedures, pooling experts from satellite and rail communities to evaluate the safety issues introduced by GNSS signals and to identify required mitigations [5]. The dominant threat for railway applications is multipath, which largely depends on the local environment where trains are travelling. Specific engineering rules are expected to position virtual balises where multipath is low enough to avoid large protection levels that might impact ERTMS performance. However, these restrictions may constrain ERTMS operations, especially in urban areas where the bounds on the maximum error of the virtual balise location may impact train operations. Obviously it has to be ensured that a train will not pass a danger point, and the additional error introduced by the location accuracy of virtual balises has to be minimized (for fixed balises, the maximum acceptable error is 5 meters). Therefore, the preferred approach is to develop an analytical model to predict and bound multipath and to mitigate anomalous multipath errors that fall outside this model. Mitigation of anomalous errors means detection by automated monitors and exclusion of affected GNSS measurements in real-time before they can corrupt train position updates at virtual balises. This methodology is being developed within the RHINOS project, where a collaboration has been established between RadioLabs and Stanford University [6].

Several technologies and signal processing techniques have been proposed in the past for mitigating the hazards produced by multipath. In this paper, we investigate a multipath monitor algorithm based on the analysis of the double differences of pseudoranges provided by two GNSS receivers connected to two separate antennas on board a single train. The rationale of our choice stems from the fact that, in the design of a hardware + software train control platform meeting highly-demanding safety constraints, train control system manufacturers usually resort to a redundant architecture and to "M-out-of-N" (MooN) combinatorial logic (typically 2oo2). In the case of GNSS based localization, to maximize the effectiveness of redundancy with respect to safety, the best engineering practices suggest the adoption of two receivers providing compatible measurements (i.e., using similar front-end filtering, code signal tracking, and carrier smoothing) but provided by different manufacturers to avoid common error modes in the software defined radio receivers.

Thus, in this paper, we exploit the peculiarities of the GNSS signals received at two different nearby sites to verify their healthiness at the end of the radiofrequency chain as well as the end of the data processing chain. Since cost effectiveness of GNSS based train localization is of primary concern, here only single-frequency (L1-only) receivers are considered, although the method can easily be extended to multiple-frequency measurements.

The proposed monitor makes use of the constraints on train motion along slowly-turning railway tracks to estimate the baseline vector between the two GNSS receiver antennas. Combining this estimate with the approximately known receiver-to-satellite geometry gives a predicted value for double-differenced receiver noise and multipath, which is compared to a threshold to determine if anomalous effects (such as unusual multipath) affecting one of the two received signals is present. The use of double differences introduces coupling of multipath effects across different monitor observables; thus a series of tests is necessary to identify the satellite most affected by multipath. This procedure is similar to that used to isolate faulty measurements identified by large "B-values" in Ground-based Augmentation Systems (GBAS). The performance of this algorithm is evaluated with and without the presence of Advanced RAIM (ARAIM) to identify scenarios where it provides additional detection capability.

This paper is organized as follows. Section 2 describes recent related work on PVT estimation for railway applications. Section 3 introduces the proposed approach for railway use, considering the case of motion constrained by railway tracks. In Section 4, experimental results based on recent field trials in Italy are presented. Finally, Section 5 provides conclusions and addresses future work.

2. TRACK CONSTRAINED DOUBLE-DIFFERENCE PVT ESTIMATE

As illustrated by Fig. 1 and Fig. 2 that report the (L1-C/A, L2-P(Y)) combination of the signals received by a GPS receiver on board a train that made the same journey at the same time on two different days, multipath is a strong phenomenon and constitutes the major source of hazard in GNSS-based railway localization. Since multipath depends on the mutual geometry among satellites, the train, and various reflecting and scattering surfaces, it tends to produce similar effects when the same geometry occurs. Thus, while hazards related to satellite ephemeris and clock errors and anomalous propagations in ionosphere and troposphere have a low occurrence probability, multipath will impair a high percentage of measurements.

Since multipath is a local phenomenon, to mitigate its impact on safety, here, in addition to the RAIM processing acting at the end of the PVT chain, we consider the adoption of a Multipath Detector and Exclusion processing scheme that benefits from the functional redundancy, at the receiver level, introduced in order to assure the integrity of the whole processing chain. This processing scheme supplements the usual monitors of signal combinations that provide evidence of multipath, such as the one shown in Figures 1 and 2. It is based on the property of the double differences among signals of a receiver pair of being affected only by thermal noise, multipath error, and RF interference, plus a deterministic component that depends on the baseline between the antenna phase centers.

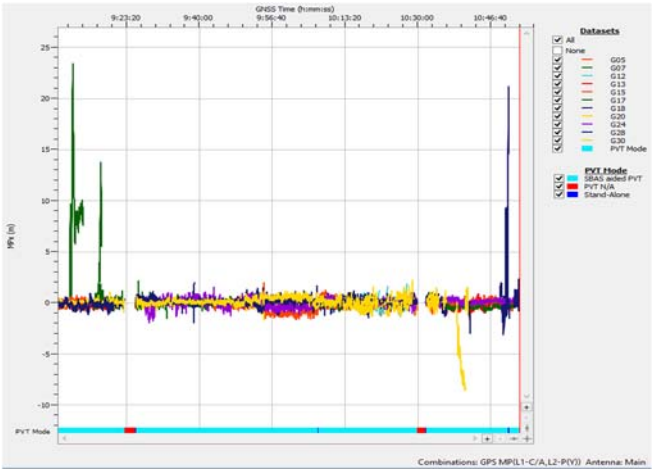

Figure 1: Analysis of multipath by Code Minus Carrier Phase Measurements

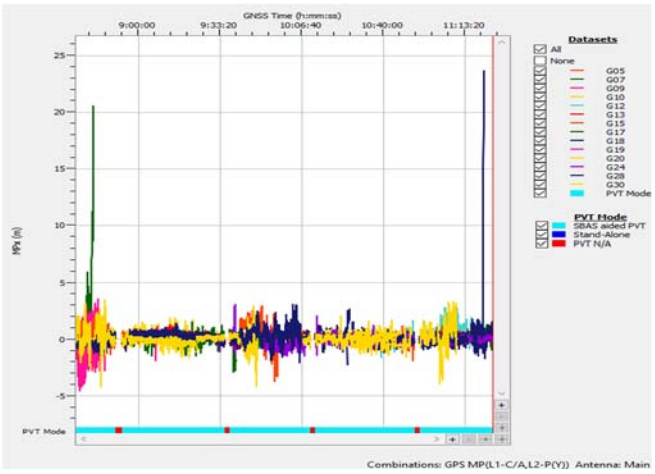

Figure 2: Analysis of multipath by Code Minus Carrier Phase Measurements in a different day for the same survey.

More specifically, let us recall that the pseudo-range $\rho^{p}_{Rx_j}(k)$ of the *p*-th satellite measured by the onboard unit (OBU) GNSS receiver Rx_j. can be expressed as (see also [7] for the details on locating a train along a known track):

$$\rho^p_{Rx_j}(k) = \left\| \mathbf{X}^p_{Sat}\left[T^p_{Sat}(k)(k)\right] - \mathbf{X}_{Rx_j}\left[T^p_{Rx_j}(k)\right] \right\| + \\ + c\Delta\tau^p_{ion,Rx_j}(k) + c\Delta\tau^p_{trop,Rx_j}(k) + \\ + c\delta t_{Rx_j}(k) + n^p_{Rx_j}(k) + \mu^p_{Rx_j}(k) - c\delta t^p_{Sat}(k), \quad j = 1,2 \qquad (1)$$

where

- $T^p_{Sat}(k)$ is the time instant at which the signal of the *k*-th epoch is transmitted from the *p*-th satellite,
- $\mathbf{X}^p_{Sat}\left[T^p_{Sat}(k)\right]$ is the coordinate vector of the *p*-th satellite at time $T^p_{Sat}(k)$,
- $T^p_{Rx_j}(k)$ is the time instant at which the signal of the *k*-th epoch transmitted from the *p*-th satellite is received by the j-th receiver,
- $\mathbf{X}_{Rx_j}\left[T^p_{Rx_j}(k)\right]$ is the coordinate vector of the *j*-th receiver, at time $T^p_{Rx_j}(k)$,
- $\Delta\tau^p_{ion,Rx_j}(k)$ is the ionospheric incremental delay along the paths from the *p*-th satellite to the j-th GNSS receiver for the *k*-th epoch w.r.t. the neutral atmosphere,
- $\Delta\tau^p_{trop,Rx_j}(k)$ is the tropospheric incremental delay along the paths from the *p*-th satellite to the *j*-th GNSS receiver for the *k*-th epoch w.r.t. the neutral atmosphere,
- $\delta t^p_{Sat}(k)$ is the offset of the *p*-th satellite clock for the *k*-th epoch,
- δt_{Rx_j} is the master station receiver clock offset,
- $n^p_{Rx_j}$ is the *j*-th receiver thermal noise and eventual radio frequency interference component,
- $\mu^p_{Rx_j}$ is the multipath error component of the *j*-th receiver.

In the following we assume that the train dynamics are such that we can neglect the differences in the location of the receiver w.r.t. the arrivals of the signals from the visible satellites, so that we can approximate $\mathbf{X}_{Rx_j}\left[T^p_{Rx_j}(k)\right]$ with the average $\mathbf{X}_{Rx_j}\left[T_{Rx_j}(k)\right]$ with respect to the visible satellites, namely,

$$\mathbf{X}_{Rx_j}\left[T_{Rx_j}(k)\right] \triangleq Mean\left\{\mathbf{X}_{Rx_j}\left[T^p_{Rx_j}(k)\right]\right\} \cong \mathbf{X}_{Rx_j}\left[T^q_{Rx_j}(k)\right] \qquad (2)$$

Then, dropping the temporal index *k* for sake of compactness, and denoting with **b** the baseline between the two antennas,

$$\mathbf{b} = \mathbf{X}_{Rx_1} - \mathbf{X}_{Rx_2}, \qquad (3)$$

and denoting with $\mathbf{e}^p_{Rx_j}$ the unit (column) vector corresponding to the line-of-sight of the *p*-th satellite with respect to the *j*-th antenna (see Fig. 3):

$$\mathbf{e}^p_{Rx_j} = \frac{\mathbf{X}^p_{Sat} - \mathbf{X}_{Rx_j}}{\left\| \mathbf{X}^p_{Sat} - \mathbf{X}_{Rx_j} \right\|}, \qquad (4)$$

and observing that (see [9])

$$r^p_{Rx_2}\mathbf{e}^p_{Rx_2} = \left\langle \mathbf{b} + r^p_{Rx_1}\mathbf{e}^p_{Rx_1}, \mathbf{e}^p_{Rx2} \right\rangle \mathbf{e}^p_{Rx_2}, \qquad (5)$$

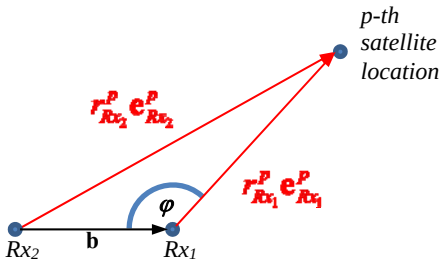

Figure 3: Two-receiver geometry to observed satellite

for the single difference SD_p between the geometric distances of the *p*-th satellite from the two receivers, we can write:

$$SD_p = \left\| \mathbf{X}^p_{Sat} - \mathbf{X}_{Rx_1} \right\| - \left\| \mathbf{X}^p_{Sat} - \mathbf{X}_{Rx_2} \right\| = \\ = r^p_{Rx_1}\left[1 - \left\langle \mathbf{e}^p_{Rx_1}, \mathbf{e}^p_{Rx_2} \right\rangle\right] - \left\langle \mathbf{b}, \mathbf{e}^p_{Rx_2} \right\rangle, \qquad (6)$$

Therefore, denoting with $DD_{p,q}$ the double difference of the pseudoranges related to the *p*-th and *q*-th satellites, we have:

$$DD_{p,q} = \left\langle \mathbf{b}, \mathbf{e}^q_{Rx_2} - \mathbf{e}^p_{Rx_2} \right\rangle + \\ + r^p_{Rx_1}\left[1 - \left\langle \mathbf{e}^p_{Rx_1}, \mathbf{e}^p_{Rx_2} \right\rangle\right] - r^q_{Rx_1}\left[1 - \left\langle \mathbf{e}^q_{Rx_1}, \mathbf{e}^q_{Rx_2} \right\rangle\right] + \nu_{p,q}. \qquad (7)$$

where $\nu_{p,q}$ is the equivalent receiver noise. For baseline lengths of a few meters, the ionospheric and the tropospheric incremental delays affecting the signal received by the two antennas are essentially identical, so that the components of the equivalent receiver noise are

$$\nu_{p,q} \cong n^p_{Rx_1} - n^p_{Rx_2} - n^q_{Rx_1} + n^q_{Rx_2} + \mu^p_{Rx_1} - \mu^p_{Rx_2} - \mu^q_{Rx_1} + \mu^q_{Rx_2}. \qquad (8)$$

On the other hand, for $r^p_{Rx_1} \cong 20,200km$ and $\|\mathbf{b}\| \le 100m$

$$\left| r^p_{Rx_1}\left[1 - \left\langle \mathbf{e}^p_{Rx_1}, \mathbf{e}^p_{Rx_2} \right\rangle\right] \right| \le 2.4\times10^{-7} m \qquad (9)$$

Therefore, the double difference $DD_{p,q}$ can be written as:

$$DD_{p,q} \cong \left\langle \mathbf{b}, \mathbf{e}^q_{Rx_2} - \mathbf{e}^p_{Rx_2} \right\rangle + \nu_{p,q}. \qquad (10)$$

If the receiver position were known, the above equations could be employed to estimate the noise double difference. On the other hand, the rate of change of the baseline orientation cannot be too large in order to avoid train derailment. Thus, a reliable prediction of the baseline at the k-th epoch can be obtained by combining the baseline estimate at the epoch (*k*-1) with the distance travelled by the train provided by the onboard odometry. Thus, denoting with $\hat{\mathbf{b}}_{k/k-1}$ the baseline at the *k*-th epoch predicted on the basis of the GNSS measurements up to the (*k*-1)-th epoch and of the travelled distance provided by the odometry, we can estimate the double difference of the receiver noise as

$$\hat{v}_{p,q} = DD_{p,q} - \left\langle \hat{\mathbf{b}}_{k/k-1}, \mathbf{e}^q_{Rx_2} - \mathbf{e}^p_{Rx_2} \right\rangle . \quad (11)$$

The previous equation can be written in matrix form, as follows:

$$\hat{\mathbf{v}}^{(p)} = \mathbf{DD}^{(p)} + \mathbf{S}^{(p)} \mathbf{e}^T_{Rx_2} \hat{\mathbf{b}}_{k/k-1} \quad (12)$$

where

$$\mathbf{e}_{Rx_j} = \left[\mathbf{e}^1_{Rx_j} \quad \mathbf{e}^2_{Rx_j} \quad \dots \quad \mathbf{e}^{N_{sat}}_{Rx_j} \right], \quad (13)$$

$\mathbf{S}^{(p)}$ is the partitioned matrix

$$\mathbf{S}^{(p)} = \begin{bmatrix} -\mathbf{I}_{p-1} & \mathbf{1}_{p-1} & 0 \\ 0 & \mathbf{1}_{N_{Sat}-p} & -\mathbf{I}_p \end{bmatrix}, \quad (14)$$

where $\mathbf{I}_M$ denotes the identity matrix of size *M*, $\mathbf{1}_M$ is a column vector of size $M \times 1$ with elements equal to 1, $\mathbf{DD}^{(p)}$ is the array

$$\mathbf{DD}^{(p)} = \left[\mathbf{S}^{(p)} \quad -\mathbf{S}^{(p)} \right] \begin{bmatrix} \boldsymbol{\rho}_{Rx_1} \\ \boldsymbol{\rho}_{Rx_2} \end{bmatrix}, \quad (15)$$

and $\boldsymbol{\rho}_{Rx_j}$ is the column array of the pseudoranges measured by the *j*-th receiver:

$$\boldsymbol{\rho}_{Rx_j} = \begin{bmatrix} \rho^1_{Rx_j} \\ \rho^2_{Rx_j} \\ \vdots \\ \rho^{N_{Sat}}_{Rx_j} \end{bmatrix}. \quad (16)$$

We observe that, denoting with

$$\mathbf{R}_{n_{Rx_j}} = diag\left(\sigma^2_{n^1_{Rx_j}}, \sigma^2_{n^2_{Rx_j}}, ..., \sigma^2_{n^{N_{sat}}_{Rx_j}} \right) \quad (17)$$

the covariance matrix of the receiver noise, the covariance of the equivalent noise double difference is:

$$\mathbf{R}_{\mathbf{v}^{(p)}} = \left[\mathbf{S}^{(p)} \quad -\mathbf{S}^{(p)} \right] \begin{bmatrix} \mathbf{R}_{n_{Rx_1}} & 0 \\ 0 & \mathbf{R}_{n_{Rx_2}} \end{bmatrix} \left[\mathbf{S}^{(p)} \quad -\mathbf{S}^{(p)} \right]^T . \quad (18)$$

3. MULTIPATH DETECTION

Multipath detection can be performed by applying thresholds to the statistics of $\hat{\mathbf{v}}^{(p)}$ from (12). Note that the use of the double difference implies that only the difference between the multipath errors affecting the two receivers can be measured. Therefore, the distance between the two antennas should be large enough to guarantee that the multipath affecting the two receivers is uncorrelated.

In the following three subsections, detectors based on the magnitude of the average of $\hat{\mathbf{v}}^{(p)}$, on the rank order statistics of the magnitude of the components of $\hat{\mathbf{v}}^{(p)}$, and of the L^2 norm of $\hat{\mathbf{v}}^{(p)}$ are illustrated.

a) Double Difference Average detector

The average detector compares the magnitude of the average $\xi^{(p)}$ of $\hat{\mathbf{v}}^{(p)}$ with a threshold γ. If the threshold is exceeded, the p-th satellite pseudorange is assumed to be significantly affected by multipath and is excluded from PVT computation.

Considering that

$$\xi^{(p)} = \frac{1}{(N_{Sat}-1)} \mathbf{1}^T_{N_{sat-1}} \hat{v}^{(p)} \quad (19)$$

the probability of a false warning of significant multipath (when conditions are actually normal) is given by

$$P_{fw} = erfc\left[\frac{\gamma}{\sqrt{2}\sigma_{\xi^{(p)}}} \right] \quad (20)$$

where

$$erfc(y) = \frac{2}{\sqrt{\pi}} \int_y^\infty e^{-t^2} dt \quad (21)$$

and

$$\sigma^2_{\xi^{(p)}} = \frac{1}{(N_{sat}-1)^2} \mathbf{1}^T_{N_{sat}-1} \mathbf{R}_{\mathbf{v}} \mathbf{1}_{N_{sat}-1} \quad (22)$$

Thus, according to the Neyman-Pearson criterion, the threshold is set as follows

$$\gamma = \sqrt{2}\sigma_{\xi^{(p)}} erfc^{-1}\left[P_{fw} \right]. \quad (23)$$

On the other hand, the probability of detecting an anomalous multipath reflection with amplitude μ affecting one of the two receivers is:

$$\breve{P}_D = \frac{1}{2} erfc\left[\frac{\gamma + |\mu|}{\sqrt{2}x\sigma_{\xi^{(p)}}}\right] + \frac{1}{2} erfc\left[\frac{\gamma - |\mu|}{\sqrt{2}\sigma_{\xi^{(p)}}}\right]. \quad (24)$$

Table I – Multipath Detection and Exclusion Procedure

a. Initialize the set $S^{Healthy}$ of healthy satellites to the set of visible satellites with elevation greater than the elevation mask.
b. Repeat
   - for each satellite in $S^{Healthy}$ compute the quantity $\left|\xi^{(p)}\right|$
c. Select the satellite with the largest $\left|\xi^{(p)}\right|$

$$\hat{p} = Arg\left\{\underset{p \in S^{Healthy}}{Max}\left[\left|\xi^{(p)}\right|\right]\right\}$$

d. If $\left|\xi^{(\hat{p})}\right|$ exceeds a predefined threshold γ
   - remove $\hat{p}$ from the healthy set $S^{Healthy}$
   - and mark the satellite as *unreliable*.

until $\left|\xi^{(\hat{p})}\right| > \gamma$ and $S^{Healthy}$ is non empty.

Obviously, a fault on the signal related to the *p*-th satellite code channel will affect every $\left|\xi^{(q)}\right|$. Nevertheless the contribution to $\left|\xi^{(p)}\right|$ is $(N_{sat} - 1)$ times the contribution to $\left|\xi^{(q)}\right|$. Thus, the signal generating the large values can be detected by selecting the satellite corresponding to the largest $\left|\xi^{(q)}\right|$.

To avoid the condition where a large fault in a signal may mask a smaller fault on another signal, the iterative procedure reported in Table I is applied. This approach removes at each iteration the effects produced by those satellites whose signal is classified as faulty. In Table I, $S^{Healthy}$ denotes the set of satellite signals classified as healthy.

b) Rank Order Statistics Detector

Let $\delta_{p,q}$ be the binary variable equal to 1 when the magnitude of $\hat{v}_{p,q}$ exceeds the threshold $\tilde{\gamma}$, i.e.:

$$\delta_{p,q} = \begin{cases} 0 & for\ \left|\hat{v}_{p,q}\right| \le \tilde{\gamma} \\ 1 & otherwise \end{cases} \quad (25)$$

In addition, let N_{sat} be the number of visible satellites at a given epoch. Then, the *p*-th satellite pseudorange is considered to be severely affected by multipath if at least *K* out of (N_{sat} -1) values of $\left|\hat{v}_{p,q}\right|$ exceed the threshold $\tilde{\gamma}$. Thus, denoting with η_p a binary variable equal to 1 if the *p*-th visible satellite pseudorange is considered as severely affected by multipath, we have

$$\eta_p = \begin{cases} 1 & for \sum_{\substack{q=1 \\ q \ne p}}^{N_{sat}} \delta_{p,q} \ge K \\ 0 & otherwise \end{cases} \quad (26)$$

With respect to multipath detector performance, we observe that, denoting with $B_{k,n}(P)$ the binomial distribution

$$B_{k,n}(P) = \binom{n}{k} P^k (1-P)^{n-k} \quad (27)$$

We obtain for the probability of False Alarm:

$$P_{fa} = \sum_{k=K}^{N_{sat}-1} B_{k,N_{sat}-1}\left(\tilde{P}_{fw}\right) \quad (28)$$

However, the detection probability is much more complex.

Let **S** be the set of the *M* visible satellites at any given epoch, and let $\mathbf{S}_k$ be set of the *k*-combinations of *k* satellites out of *M*

$$\mathbf{S}_{k,N_{sat}} = \left\{ s_{k,m}^{N_{sat}} \middle| m = 1, \ldots, \binom{m}{N_{sat}} \right\} \quad (29)$$

where $s_{k,m}^{N_{sat}}$ is the *m*-th *k*-combination. In addition let us denote with $\overline{s}_{k,m}^{N_{sat}}$ the complementary set of satellites with respect to $s_{k,m}^{N_{sat}}$.

Then, assuming without loss of generality that the visible satellite set is reordered in such a way that the satellite pseudorange for which anomalous multipath has to be verified is the last of the collected set of satellites, we have:

$$P_D = \sum_{k=K}^{N_{sat}-1} \sum_{m=1}^{\binom{N_{sat}-1}{k}} \prod_{n_1 \in s_{k,m}^{N_{sat}-1}} \tilde{P}_D\left(\tilde{b}_{N_{sat},n_1}\right) \prod_{n_2 \in \overline{s}_{k,m}^{N_{sat}-1}} \left[1 - \tilde{P}_D\left(\tilde{b}_{N_{sat},n_2}\right)\right] \quad (30)$$

Based on (27), we observe that the detection capability decreases with the antenna baseline magnitude.

c) L^2 norm detector

In this case, multipath detection is performed by comparing the L^2 norm $\zeta^{(p)}$ of $\hat{\mathbf{v}}^{(p)}$:

$$\zeta^{(p)} = \left[\hat{\mathbf{v}}^{(p)}\right]^T \hat{\mathbf{v}}^{(p)} \tag{31}$$

with a threshold $\tilde{\gamma}$.

Obviously, the procedure described in Table I can be immediately extended to $\zeta^{(p)}$ thresholding. When there is no multipath, $\zeta^{(p)}$ is a random variable with a generalized central chi-square distribution with $N_\zeta = N_{sat} - 1$ degrees of freedom. Let us denote with $D_{G\chi^2_n}(x;\boldsymbol{\Lambda})$ the generalized chi-square central distribution with *n* degrees of freedom:

$$D_{G\chi^2_n}(x;\boldsymbol{\Lambda}) = \frac{1}{\prod_{i=2}^{n}\Lambda_i} D_{\chi^2_1}\left(\frac{x}{\Lambda_1}\right) * p_{\chi^2_1}\left(\frac{x}{\Lambda_2}\right) * \ldots * p_{\chi^2_1}\left(\frac{x}{\Lambda_n}\right) \tag{32}$$

where $D_{\chi^2_n}(\cdot)$ is the cumulative chi square distribution with *n* degrees of freedom, and $p_{\chi^2_n}(\cdot)$ is the corresponding probability density function. $\boldsymbol{\Lambda}$ is the vector:

$$\boldsymbol{\Lambda} = \begin{bmatrix}\Lambda_1 & \Lambda_2 & \ldots & \Lambda_n\end{bmatrix}^T, \tag{33}$$

and $*$ denotes convolution. Then the probability of incorrectly excluding the *n*-th healthy satellite pseudorange is

$$P_{fw}^{L^2} = 1 - D_{G\chi^2_{N_z}}\left(\tilde{\gamma};\boldsymbol{\Lambda}_{\zeta^{(p)}}\right), \tag{34}$$

where $\boldsymbol{\Lambda}_{\zeta^{(p)}}$ is the vector of the eigenvalues of $\mathbf{R}_{\mathbf{v}^{(p)}}$.

On the other hand, when the pseudoranges of the *p*-th satellite observed by the two receivers are affected by multipath with amplitudes η_1 and η_2, $\hat{\mathbf{v}}^{(p)}$ can be written as

$$\mathbf{v}^{(p)} = \begin{bmatrix}\mathbf{S}^{(p)} & -\mathbf{S}^{(p)}\end{bmatrix}\begin{bmatrix}\mathbf{G}_1 & \mathbf{0}\\ \mathbf{0} & \mathbf{G}_2\end{bmatrix}\begin{bmatrix}\mathbf{u}_1\\ \mathbf{u}_2\end{bmatrix} \tag{35}$$

where

$$\mathbf{G}_j = diag\left(\sigma_{n_1^{Rx_j}}, \sigma_{n_2^{Rx_j}}, \ldots, \sigma_{n_{N_{sat}}^{Rx_j}}\right) \tag{36}$$

and $\mathbf{u}_1$ and $\mathbf{u}_2$ are two independent Gaussian random variables with independent components with unit variance and expectations $\mathbf{G}_j^{-1}\boldsymbol{\beta}_j$, where

$$\beta_j = \begin{bmatrix}0\\ \vdots\\ \eta_j\\ \vdots\\ 0\end{bmatrix} \leftarrow p-th\ row \qquad j = 1,2. \tag{37}$$

Let $\boldsymbol{\Gamma}\boldsymbol{\Lambda}\boldsymbol{\Gamma}^T$ be the spectral decomposition of

$$\begin{bmatrix}\mathbf{G}_1^T & 0\\ 0 & \mathbf{G}_2^T\end{bmatrix}\begin{bmatrix}\left[\mathbf{S}^{(p)}\right]^T\\ -\left[\mathbf{S}^{(p)}\right]^T\end{bmatrix}\begin{bmatrix}\mathbf{S}^{(p)} & -\mathbf{S}^{(p)}\end{bmatrix}\begin{bmatrix}\mathbf{G}_1 & 0\\ 0 & \mathbf{G}_2\end{bmatrix}$$

so that we can write

$$\begin{bmatrix}\mathbf{G}_1^T & 0\\ 0 & \mathbf{G}_2^T\end{bmatrix}\begin{bmatrix}\left[\mathbf{S}^{(p)}\right]^T\\ -\left[\mathbf{S}^{(p)}\right]^T\end{bmatrix}\begin{bmatrix}\mathbf{S}^{(p)} & -\mathbf{S}^{(p)}\end{bmatrix}\begin{bmatrix}\mathbf{G}_1 & 0\\ 0 & \mathbf{G}_2\end{bmatrix} = \boldsymbol{\Gamma}\boldsymbol{\Lambda}\boldsymbol{\Gamma}^T \tag{38}$$

Then, $\zeta^{(p)}$ can now be written as

$$\begin{aligned}\zeta^{(p)} &= \left[\hat{\mathbf{v}}^{(p)}\right]^T \hat{\mathbf{v}}^{(p)} = \\ &= \mathbf{u}^T\boldsymbol{\Gamma}\boldsymbol{\Lambda}\boldsymbol{\Gamma}^T\mathbf{u} = \\ &= \mathbf{x}^T(k)\boldsymbol{\Lambda}\mathbf{x}(k) = \\ &= \sum \Lambda_h x_h^2\end{aligned} \tag{39}$$

where x_h^2 are independent non-central chi-square random variables with non-centrality parameter μ_h^2, where $\boldsymbol{\mu}$ is the expectation of $\mathbf{x}$, for which we have

$$\boldsymbol{\mu} = \boldsymbol{\Gamma}^T\mathbf{G}^{-1}\boldsymbol{\beta}_n^i(k) \tag{40}$$

Thus, denoting with $D^{nc}_{G\chi^2_n}(x;\boldsymbol{\Lambda},\boldsymbol{\mu})$ the generalized chi-square central distribution with *n* degrees of freedom:

$$\begin{aligned}D^{nc}_{G\chi^2_n}(x;\boldsymbol{\Lambda},\boldsymbol{\mu}) &= \frac{1}{\prod_{i=2}^{n}\Lambda_2} \times \\ &D^{nc}_{\chi^2_1}\left(\frac{x}{\Lambda_1},\frac{\mu_1^2}{\Lambda_1^2}\right) * p^{nc}_{\chi^2_1}\left(\frac{x}{\Lambda_2},\frac{\mu_2^2}{\Lambda_2^2}\right) * \ldots * p^{nc}_{\chi^2_1}\left(\frac{x}{\Lambda_n},\frac{\mu_n^2}{\Lambda_n^2}\right)\end{aligned} \tag{41}$$

where $D^{nc}_{\chi^2_n}\left(\cdot;\mu^2\right)$ is the cumulative non-central chi-square distribution with *n* degrees of freedom and non-centrality parameter μ^2, and $p^{nc}_{\chi^2_n}\left(\cdot;\mu^2\right)$ is the corresponding probability density function, *the probability of Missed Exclusion of a faulty signal based on the test performed on* $\zeta^{(p)}$ is given by:

$$P_{ME,\zeta^{(p)}}(\beta) = D^{nc}_{\chi^2_{N_\zeta}}\left[\underset{\sim}{\gamma};\Lambda,\Gamma^T\mathbf{G}^{-1}\boldsymbol{\beta}\right]. \tag{42}$$

Numerical evaluation of the Missed Exclusion probability can be performed in the statistical computing language "R" by means of the "CompQuadForm" software package, which is available at https://cran.r-project.org/web/packages/CompQuadForm/index.html.

4. EXPERIMENTAL RESULTS

The described multipath detectors have been tested on a data set acquired during a test campaign performed under the framework of the ESA Artes 20 3InSat project on the Pontremolese line in Northern Italy (see Figure 4). In the past, a large number of physical balises have been deployed along this line for test purposes (about 500 along a total length of about 120 km). Thus, GNSS observations can be complemented with a very accurate reference trajectory, addressed in the following as Ground Truth, built by post-processing odometry and the physical balise readings that provide precise positioning of the train at the time of passage over each balise.

Figure 4: Pontremolese line in Northern Italy.

Figure 5: Electric traction ALe.642 trains.

For the test campaign, 3 Remote Integrity Monitor (RIM) stations, each equipped with two low-cost GPS receivers from two different manufacturers, were deployed along the track wayside, while two electric traction trains of type ALe.642 (see Figure 5), each equipped with two GPS receivers of the same kind of those utilized for the RIM stations, were employed. As illustrated by Figure 6, the Pontremolese line is a rather challenging environment with respect to multipath due to the large number of tunnels, overpasses, and sky occlusions.

Figure 6: Pontremolese line observation environment

In Figures 7 through 21, the results from a run from La Spezia to Pontremoli are reported. In Figure 7, the magnitude of the average $\xi^{(p)}$ of $\hat{\mathbf{v}}^{(p)}$ for the satellites in view is reported. According to the algorithm of Table I, for each epoch, the satellite corresponding to the largest absolute mean is removed from the list of visible satellites whenever that value exceeds the detection threshold. As illustrated by Figure 8 and Figure 9, the update of $\left|\xi^{(p)}\right|$ after measurement removal may show evidence of the presence of additional satellites affected by multipath. Thus, successive checks of the largest absolute mean and removal of visible satellites that exceed the threshold is recursively applied until the revised values of $\left|\xi^{(p)}\right|$ for all remaining satellites no longer exceed the threshold. Figures 10, 11, 12 illustrate the same process for the L^2 norm test statistic $\zeta^{(p)}$.

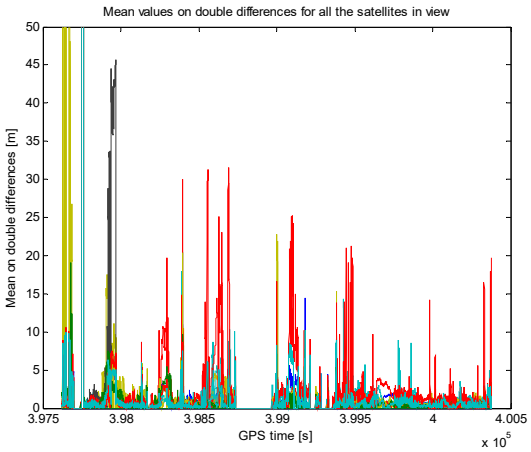

Figure 7: First Iteration: mean values of the double differences for all (non-excluded) satellites in view.

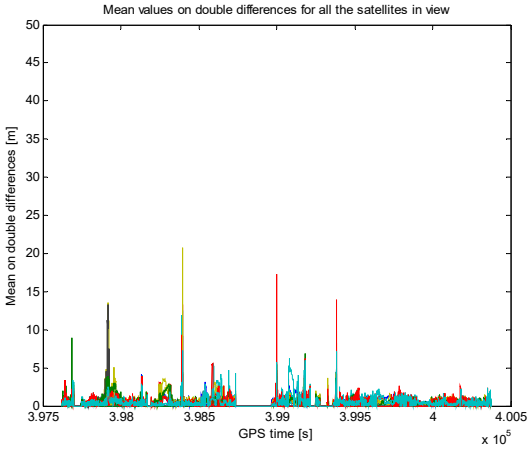

Figure 8: Second Iteration: mean values of the double differences for all (non-excluded) satellites in view.

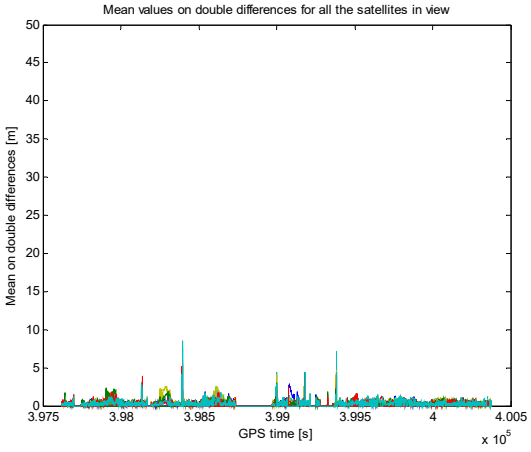

Figure 9: Third Iteration: mean values of the double differences for all (non-excluded) satellites in view.

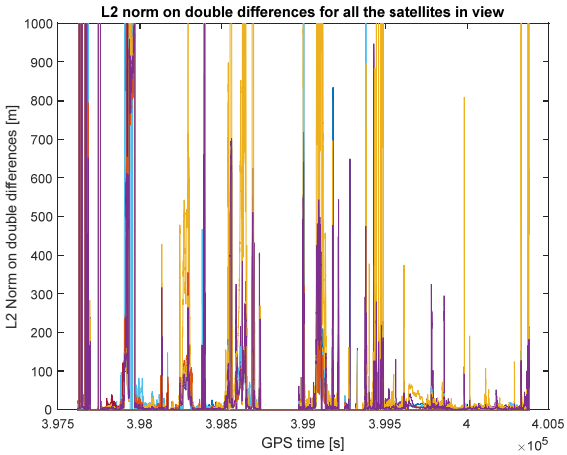

Figure 10: First Iteration: L2 norm values of the double differences for all (non-excluded) satellites in view.

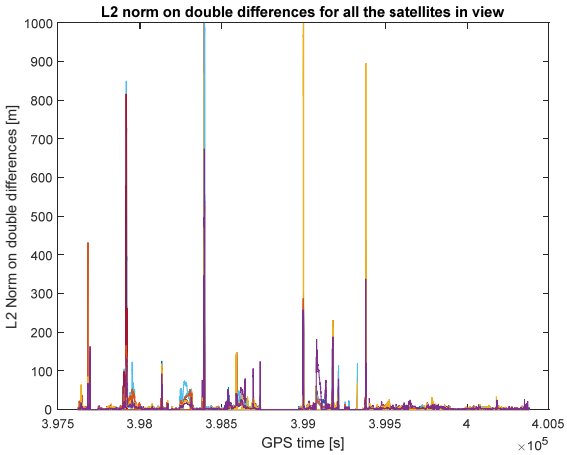

Figure 11: Second Iteration: L2 norm values of the double differences for all (non-excluded) satellites in view.

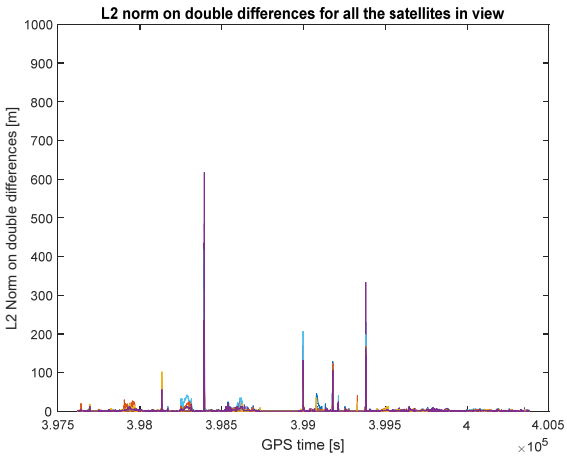

Figure 12: Third Iteration: L2 norm values of the double differences for all (non-excluded) satellites in view.

The impact of satellite removal on system performance is shown by Figure 13 (without detection and exclusion) and Figure 14 (with detection and exclusion), where the error in the estimated train mileage (in meters) is plotted. Since the train mileage is obtained by fusing the estimates produced by the two receivers, large errors on a single receiver are filtered out during this comparison. Thus, the effect of the multipath detection and exclusion algorithm is an increase in the number of epochs for which the estimated location is considered to be valid. This effect is evidenced by comparison to Figures 15 through 18, where the mileage errors corresponding to the individual receivers are reported.

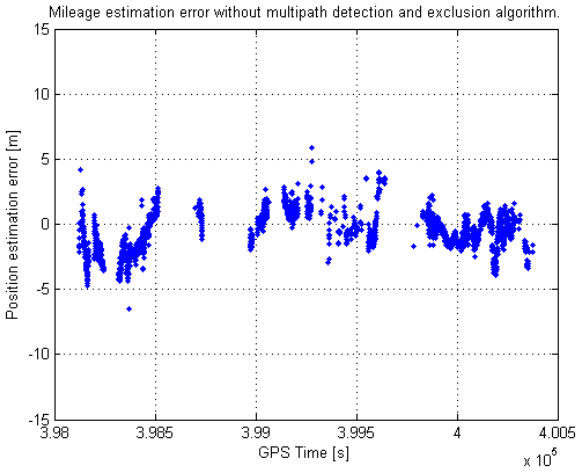

Figure 13: Mileage estimation error without multipath detection and exclusion algorithm.

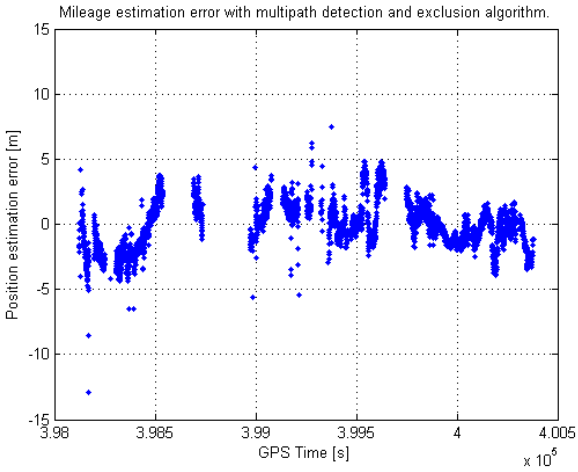

Figure 14: Mileage estimation error when multipath detection and exclusion algorithm is applied.

The two estimates of the train mileage provided by the two receivers are considered to be coincident (2oo2 logic) if the magnitude of their difference falls below a threshold γ_F. This threshold can be set by observing that, when there is no multipath, the mileage error can be overbounded by a zero

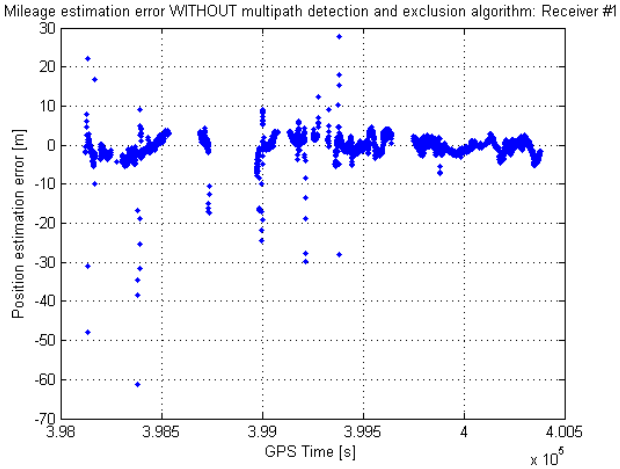

Figure 15: Mileage estimation error without multipath detection and exclusion algorithm for Receiver #1.

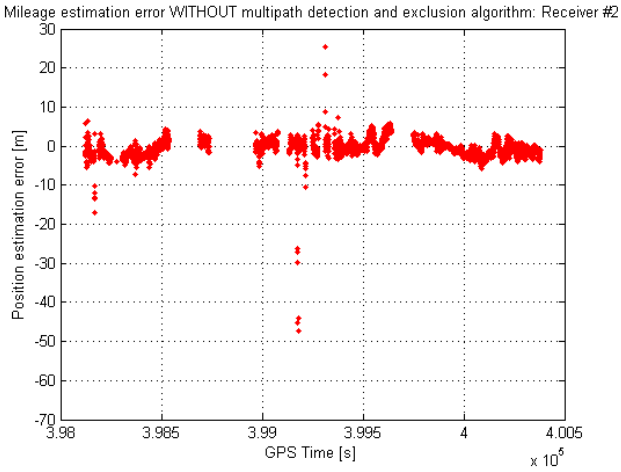

Figure 16: Mileage estimation error without multipath detection and exclusion algorithm for Receiver #2.

mean Gaussian distribution with variance $\sigma_{s_i}^2$. Thus the probability of incorrectly discarding a good estimate is

$$P_{FE} = erfc\left[\frac{\gamma_F}{\sqrt{2\left(\sigma_{s_1}^2 + \sigma_{s_2}^2\right)}}\right] . \qquad (43)$$

The impact of multipath detection and exclusion on the mileage estimate of a single receiver can be appreciated from Figure 17, where the error of Receiver #1 (with detection and exclusion activated) is depicted. Figure 18 shows the same result for receiver #2.

The fact that improving the estimate produced by one receiver increases the number of epochs for which the estimate is considered to be valid is even more evident in the Stanford triangle diagrams in Figure 19 and Figure 20 that

plot mileage error (the difference between estimated mileage from the GNSS-based system and actual mileage determined by the physical balise system) on the *x*-axis and the computed protection level on mileage error on the *y*-axis. Figure 19 shows the result without multipath detection and exclusion, while Figure 20 shows the result with multipath detection and exclusion based on the double-difference average detector described in Section 3(a). These plots show an increase of about 2.4 % in system availability (from 71.4% to 73.8%) when multipath detection and exclusion is applied. We remark that these results are for a single constellation (GPS only) and will improve when other satellite constellations are used with GPS.

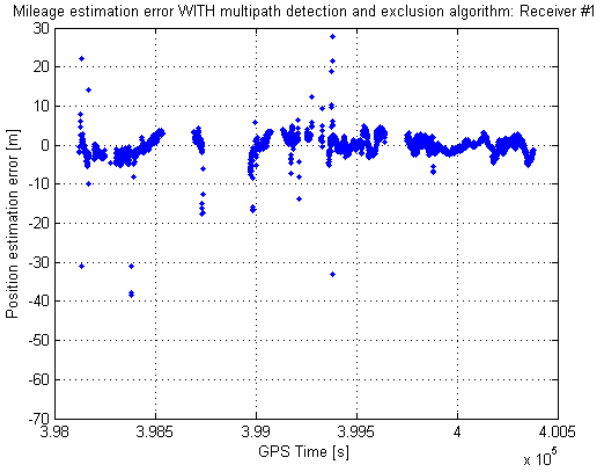

Figure 17: Mileage estimation error with multipath detection and exclusion algorithm for Receiver #1

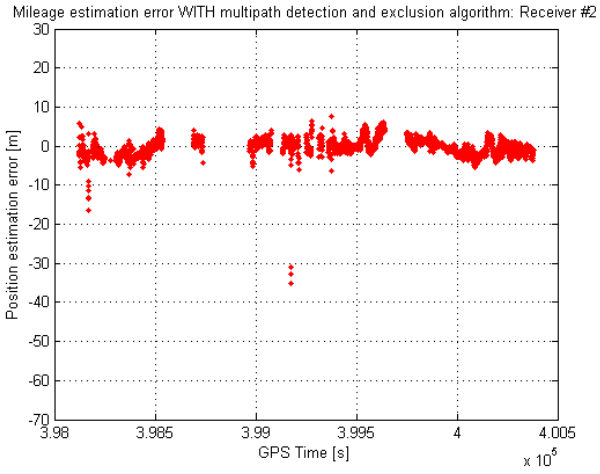

Figure 18: Mileage estimation error with multipath detection and exclusion algorithm for Receiver #2

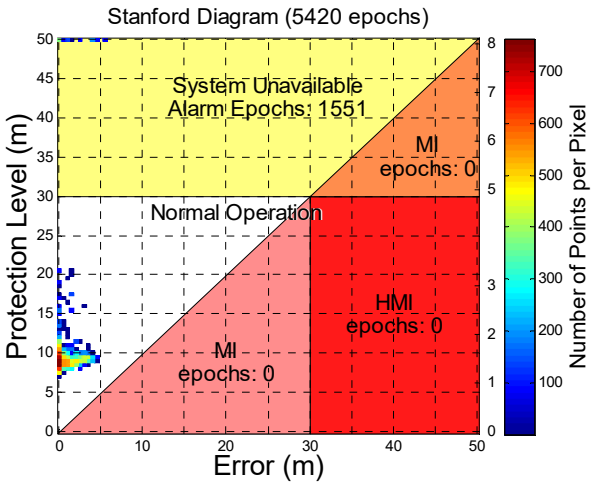

Figure 19: Stanford triangle plot. No Multipath detection and exclusion algorithm is applied.

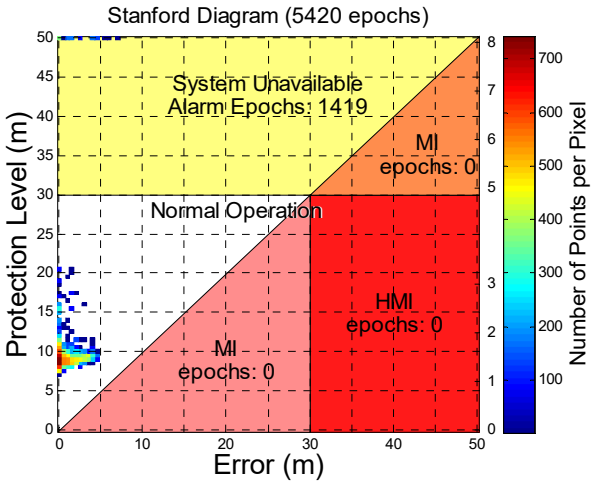

Figure 20: Stanford triangle plot. Multipath detection and exclusion algorithm based on Double Difference average.

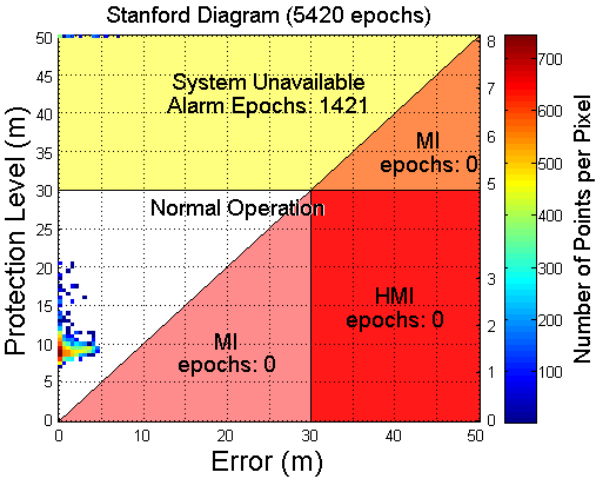

Figure 21: Stanford triangle plot. Multipath detection and exclusion algorithm based on L^2 norm.

As illustrated by comparing Figure 20 with Figure 21, where the Stanford triangle plot for the multipath detector based on L^2 norm thresholding is shown, there is no significant difference in the performance of the double-difference average detector in Figure 20 and the L^2 norm detector in Figure 21.

Furthermore, along this railway, tunnels with no sky visibility and other regions with limited sky visibility exist. In these cases, as evidenced by Figure 22, satellite exclusion can lead to a drastic reduction in the number of visible satellites. In particular, this value can drop below the minimum number of satellites required for position fixing. Even when the number of satellites stays just above this level, the protection levels are relatively high due to poor positioning geometry. Therefore, as noted earlier, the use of multiple constellations is important to increasing availability over what is shown in these results.

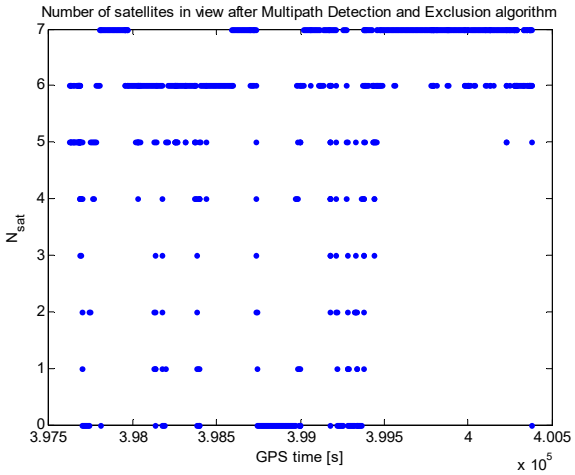

Figure 22: Number of GPS satellites used for PVT estimation after Multipath and Exclusion algorithm.

CONCLUSIONS AND FUTURE WORK

Satisfying the highly demanding integrity requirements in harsh environments such as the railways lines where the ERTMS standard is being operated, requires to minimize the multipath effect that is the dominant hazard in railways domain. The method proposed in this paper supported by experimental results demonstrate that significant mileage error reduction can be obtained by coupling the 2oo2 logic acting at the end of the GNSS LDS chain, with a preliminary check on the quality of the received signal in the presence of multipath. This approach fully exploits both dual receiver redundancy and knowledge of the georeferenced railway location.

The results in this paper demonstrate the capabilities of real-time assessment of the integrity of received signals based on the statistics of the double differences of the signals received by two antennas onboard the train. In addition, exploitation of the fact that similar situations arise as soon as the mutual geometry between satellites and receivers is repeated can be utilized to build a map of the multipath characteristics along a railway. This is important information to use as a guideline when selecting the locations of virtual balises, as these balises should be located where multipath is limited and its errors are easily bounded. In this respect, an overbounded 5m error, that is the residual error of the odometer after the recalibration with a phisical balise, represents a target value to achieve with GNSS to generate virtual balises and to minimize the impacts on the mission profile. Higher errors can be managed but at a price to modify the mission operations. Track discrimination is more demanding (about 3m) for Starting of Mission in ERTMS operating scenarios. Here the challenge for GNSS is to identify the track occupied by the train with the train in stand still mode in order that a movement authority can be given directly in full supervision, saving time and improving safety.In fatc, today Start of Mission is performed under the driver responsibility with a limited speed until a balise is captured to know in which track the train is. Other parameters are the availability of the bounded error, that impacts on the ERTMS operations, and the interoperability requirement which means that virtual balises (as physical balises) have to behave “transparently” respect to on board units of different manufacturers.

Since the train environment shares many properties with the automotive one, when urban scenarios are considered, future work will consider the extension of the method described here to automotive applications. In the short term, railways are in pole position to lead the adoption of GNSS in regulated and safety relevant applications, but in the longer term autonomous vehicles will drive the self-positioning technologies that are beneficial also for the rail domain.

ACKNOWLEDGEMENTS

The authors wish to thank the team of RFI (F. Senesi, M. Ciaffi, and D. Caronti) for the test campaign and for technical support and guidance during the data analyses.

REFERENCES

[1] 2015 PTC Annual Report https://www.fra.dot.gov/Page/P0628

[2] The ERTMS Roadmap and the Future Role of ERA ERTMS CCRCC Conference 2015.Josef DOPPELBAUER, Executive Director Lille, 22 September 2015

[3] B.J.Sterner, On the Method of combining GPS and ETCS for Localization Purposes. 8th May 1998, ERRI

[4] F.Senesi, ERSAT: ERTMS + Satellite. Workshop ERSAT – Rome, Italy 16th February 2106

[5] L.Guerrucci, "Activity on Risk Analysis for the Introduction of satellite technologies for ERTMS L2", CIFI Conference, Cagliari, Italy 26th May 2016

[6] Filip, A., Beugin, J., Marais, J. "Safety Concept of Railway Signalling Based on Galileo Safety-of-Life Service," COMPRAIL, Toledo, Spain, Sept 15-17, 2008, pp. 103-112.

[7] Neri, A., Filip, A., Rispoli, F., Vegni, A. M., "An Analytical Evaluation for Hazardous Failure Rate in a Satellite-based Train Positioning System with reference to the ERTMS Train Control Systems", ION 2012, Nashville, 2012.

[8] A. Neri, S. Sabina, U. Mascia, "GNSS and odometry fusion for high integrity and high available train control systems", ION GNSS+ 2015, Tampa, FL, U.S.A;

[9] A. Neri, V. Palma, F. Rispoli and A. Vegni, "Track Constrained PVT Estimation based on the Double-Difference Technique for Railway Applications," in *Proc. of EUSIPCO 2013, September 9-13, 2013, Marrakech, Morocco*, Marrakech, Morocco, September 9-13, 2013.